Magnetic mirror effects on a collisionless plasma in a convergent geometry

Manuel Martínez-Sánchez[1] and Eduardo Ahedo[2]
[1]*Massachusetts Institute of Technology, 77 Massachusetts Avenue,
Cambridge, Massachusetts 02139-4307, USA*
[2]*Universidad Politécnica de Madrid, Madrid 28040, Spain*

Several plasma thruster concepts, as well as ion engine chambers, use magnetic cusps to protect walls and to throttle electron flow to anodes. We present a kinetic model of the plasma in the vicinity of one cusp. Electrons, strongly confined by the electrostatic presheath and sheath, are assumed isotropic. Collisionless ions are either magnetically guided or completely nonmagnetized, thus bracketing conditions of interest. For magnetized ions, electrostatic and magnetic mirror forces compete, and the resulting self-consistent potential is found by imposing quasineutrality. A similar competition occurs for nonmagnetized ions, this time as a result of the convergence of equipotential lines. Analytical solutions are found for monoenergetic ions, and these are generalized to the case of an initially Maxwellian population, for which some numerical iteration is required. The presheath potential drop is in all cases of the order of 0.6–0.75 times the electron temperature, and ions enter the sheath at a sonic velocity, according to Bohm's criterion. Contrary to intuition, the cusp does not reduce the ion flux (per unit area) to the wall, only the size of the wall area section that carries this flux by virtue of its connection to the distant plasma. These kinetic results are verified by checking the conservation of relevant moments of the ion distribution, including two new quantities that generalize the average magnetic moment and the total ion enthalpy by accounting for the nonzero ion heat fluxes. © *2011 American Institute of Physics*. [doi:10.1063/1.3554650]

I. INTRODUCTION

This work is motivated by the current research work on the divergent cusped-field thruster (DCFT)[1–5] and the related concepts cylindrical hall thruster (CHT)[6,7] and HEMP.[8,9] In these devices, particularly in DCF and HEMP, strong linear magnetic cusps are provided, running azimuthally at one or more axial locations. In DCFT and CHT there is also a central axisymmetric cusp, which in the case of the DCFT leads to the central anode location. Azimuthally running magnetic cusps are also characteristic of most Kaufman-type ion engine ionization chambers, and they tend to be collocated with the ring anode.[10]

Figure 1(a) shows the magnetic configuration of the DCFT thruster. Notice the strong fields present near the ring cusps (order of 0.4 T) and in front of the anode (about 0.5 T). In the CHT designs, these fields tend to be lower (less than 0.1 T), although still stronger than typically seen in Hall thrusters. The surface probe data in Figs. 1(b) and 1(c) will be discussed below.

The intended roles of these cusped-field configurations are (a) to magnetically shield the thruster wall so as to minimize bombardment and erosion, and (b) to provide a restriction to the flow of electrons to the anode, thus improving current efficiency and enhancing ionization. This electron-throttling role is similar to that played by the radial $\vec{B}$ field in Hall thrusters, except that in that case the restriction occurs due to the large cross-field impedance (often limited by turbulence), while in a cusped-field configuration the restriction may be aided by magnetic mirroring effects.

Because of the ion engine applications, as well as other applications related to ion sources, there has been a fair amount of theoretical work aimed at predicting the rate of ion impingement on cusp-protected walls and the rate of electron energy loss to anodes. This is surveyed for example in Ref. 10. A commonly quoted semiempirical rule[11,12] is that the width of the ion loss channel at the cusp is a few times the so-called hybrid gyro radius

$$\rho_H = \sqrt{\rho_e \rho_i}, \tag{1}$$

where $\rho_e = m_e \bar{c}_e / eB$, with a similar definition for ρ_i, are the electron and ion gyro radii, and $\bar{c}_e$ is the electron mean thermal speed. Some theoretical substantiation for this was provided by the diffusive fluid model of Ref. 13, although the factor relating ρ_H to the loss width was also found to depend on geometrical factors specific to each discharge.

A less detailed model, in which the ion velocity was derived from order-of-magnitude arguments only, was proposed in Ref. 10, resulting in the prediction that the ion flux at the sheath entrance in front of the cusp should be reduced as the magnetic field ratio between the cusp and the "saddle point," away from the wall, is increased. This particular result is in apparent conflict with simple presheath considerations that will be discussed in more detail in this paper: if, as required for sheath formation, ions must enter the sheath near the velocity $\sqrt{kT_e/m_i}$, the potential drop from the core plasma must be of the order of $kT_e/2e$, and since the electrons are well confined, and therefore near Maxwell–Boltzmann equilibrium, the ratio of plasma densities (sheath edge/core) must be of the order of $\exp(-1/2)$. Thus, both ion velocity and density should be as they would in an ordinary presheath with no magnetic effects, and the main role of the magnetic cusp would be to limit the width of the wall region
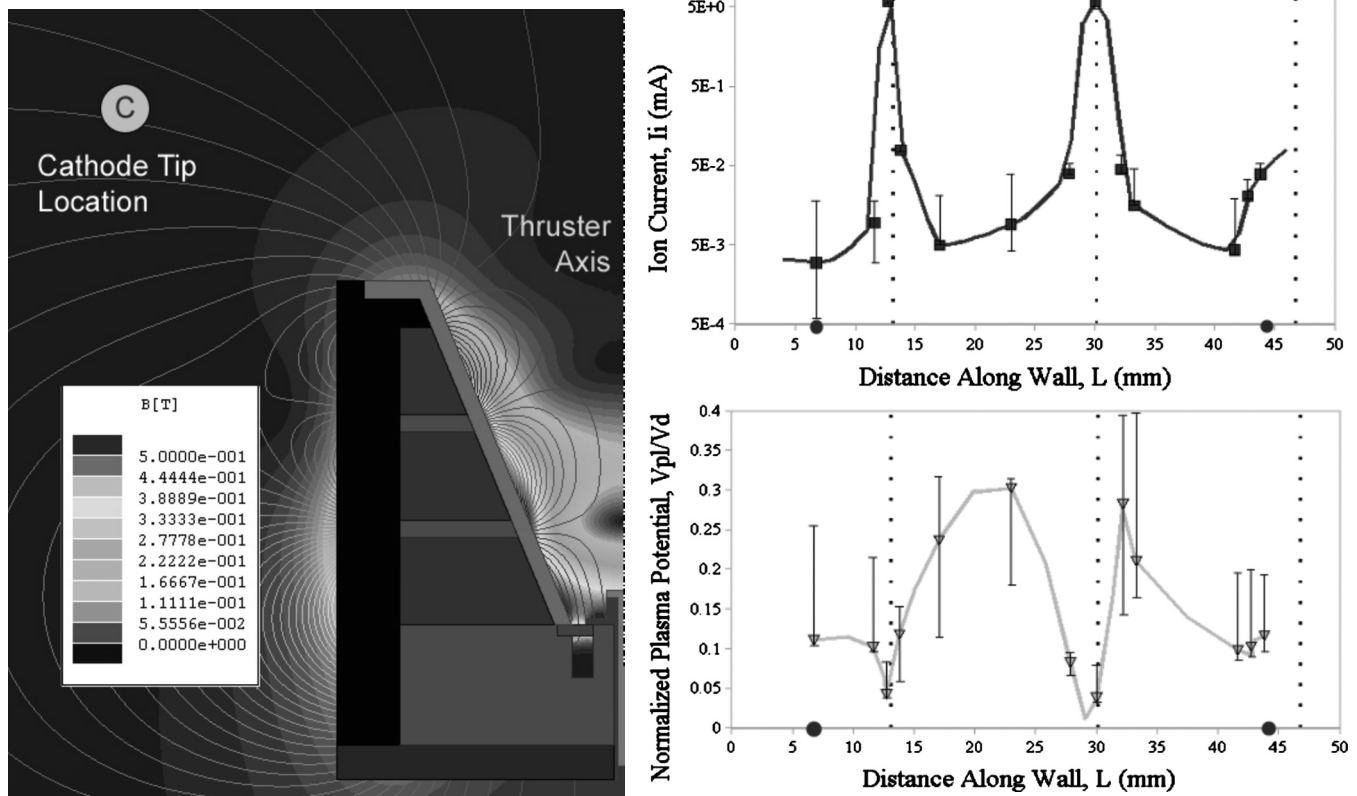
FIG. 1. (Left) Magnetic map for DCF thruster (Ref. 1). (Right-top) Ion current density at the walls, from surface probes (Ref. 5). (Right-bottom) Potential near the wall, also from surface probing (Ref. 5).

that receives this flux because points too far from the cusp axis are not connected by a magnetic line to the dense plasma far from the wall. This is supported by the experimental data of Ref. 12, for both, a ring cusp and a point-cusp, that show density and potential drops of the order of 1/2 along the cusp centerlines, as well as a strong flux reduction outside a narrow channel about these lines. Our own recent experimental data on the ion wall flux in a DCF thruster,[5] shown in Fig. 1(b), also appear to confirm this lack of a strong reduction of ion flux at the cusps, as well as its suppression between cusps.

In this paper we formulate the problem in its basic kinetic form, which yields a tractable model if collisions and cross-drifts are ignored. It is found that the ion dynamics, averaged in the cross-section of the magnetic channel, is very similar in the limiting cases of strong and weak magnetization (as long as electrons remain strongly magnetized). We present the basic formulation for magnetized ions in Sec. II, obtain analytical results for a monoenergetic population in Sec. II A and generalize this to ions that connect to a Maxwellian plasma in Sec. II B. In Sec. III we consider the leading moments of the ion distribution, and prove two new conservation laws that, for a stationary and quasi-1D flow, extend the double-adiabatic laws of Chu, Goldberger, and Low (CGL)[14] when heat fluxes are not neglected. These laws are then used to verify the results of the kinetic model, and excellent agreement is obtained. Sec. IV discusses the non-magnetized ion case and its mapping into the magnetized case.

II. KINETIC MODEL FOR STRONGLY MAGNETIZED IONS

A small Debye length collisionless plasma flows from $z < 0$ toward a wall placed at $z = 0$, with its electrons and ions guided by a convergent, quasi-one-dimensional (1D) magnetic field $B(z)$ with $dB/dz > 0$. The cross-sectional area of the convergent magnetic nozzle is $A(z)$, with

$$BA = B_S A_S,$$

where the subscript S refers to the sheath edge, or, within the model assumptions, to the wall. The cross-section $A_\infty \gg A_S$ marks the approximate bounds of the highly magnetized region. Beyond this limit, the plasma is weakly perturbed and its density n_∞ and temperatures $T_e, T_{i\infty}$ are assumed known.

The presence of the wall creates an axial electric field $E_z = -d\phi/dz$ that attracts ions toward the wall. Since the plasma response depends directly on B, and $B(z)$ is monotonic, we take B as our independent variable. The presheath ends when $d\phi/dz \to -\infty$, and the sheath is seen as a discontinuity in the quasineutral scale, i.e., $z_S \cong 0$. Electrons are strongly confined away from the wall, both electrostatically and magnetically. Then, if collisions are negligible, the electron distribution function, f_e, over most of velocity space is the same as that in the distant plasma. This excludes only those velocities away from the wall that cannot be gained by an electron with a turning point near the wall, but for normal sheath strengths, the error is quite small. If this distant

plasma is taken to be fully equilibrated and isotropic, with temperature T_e, one consequence is the applicability of the Boltzmann relation

$$n_e(\phi) = n_\infty \exp(e\phi/kT_e), \tag{2}$$

where the electron temperature is constant and *equal to its upstream value*. This means that the average kinetic energy of all electrons found at a point $P(\phi)$ with $\phi<0$ is independent of the potential, a counterintuitive result. Each electron does lose kinetic energy in moving to a lower potential, but the population at this lower potential excludes some lower energy electrons that are turned back at intermediate points; both effects cancel each other.

The isotropy of the electron distribution in the distant, unmagnetized region is a natural assumption. However, if due to details of the plasma origin, it were not isotropic, although possibly still bi-Maxwellian, with separate temperatures in the parallel and perpendicular directions, the present analysis would need revision.

The ion density $n_i(B, \phi)$ is to be obtained from the ion velocity distribution function f_i at the location where ϕ and B occur. The quasineutrality condition

$$n_e(\phi) = n_i(B, \phi) \tag{3}$$

is then an implicit equation for $\phi(B)$.

For a collisionless plasma, f_i is just a function of the ion constants of motion. A magnetized ion gyrates tightly around a magnetic line, while its gyro center translates along the line. The constants of the motion are then the ion energy E and the magnetic moment μ

$$E = \frac{m_i}{2}(w_\parallel^2 + w_\perp^2) + e\phi, \tag{4a}$$

$$\mu = \frac{m_i w_\perp^2}{2B}, \tag{4b}$$

with $w_\parallel$ and $w_\perp$ the velocity components parallel and perpendicular to $\vec{B}$, respectively. In terms of E and μ, these components are

$$w_\parallel(E, B, \mu) = \pm\sqrt{\frac{2}{m_i}[E - e\phi(B) - \mu B]}, \tag{5a}$$

$$|w_\perp(B, \mu)| = \sqrt{2\mu B/m_i}. \tag{5b}$$

Ions with $w_\parallel>0$ may reach the wall and be neutralized, or may first reach a turning point ($w_\parallel=0$) due to the magnetic mirror forces. Given E, B, and a potential distribution $\phi(B)$ (to be determined), no ions exist with μ greater than a certain limit

$$\mu_m(B, E) = \frac{E - e\phi(B)}{B}. \tag{6}$$

For small B, ϕ is near zero, and $\mu_m \cong E/B$, but near the wall, where $d\phi/dB \to -\infty$, μ_m increases steeply with B. Thus $\mu_m(B, E)$ has a minimum:
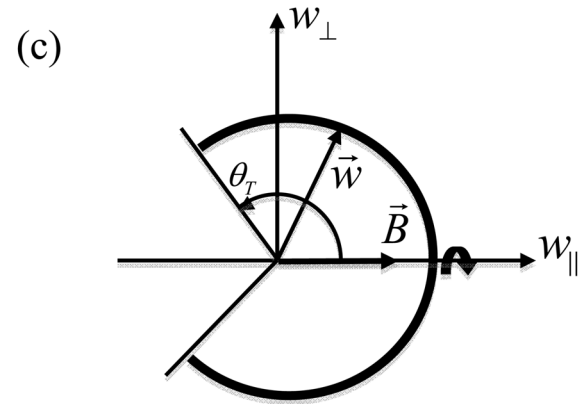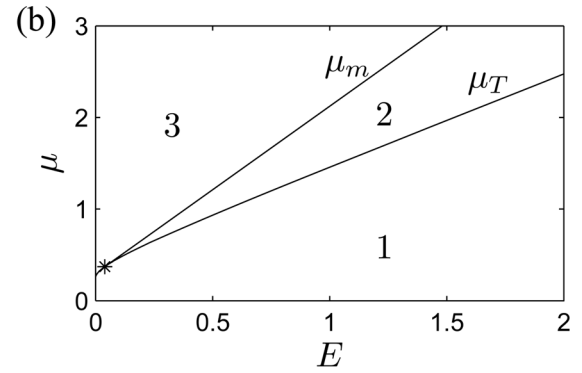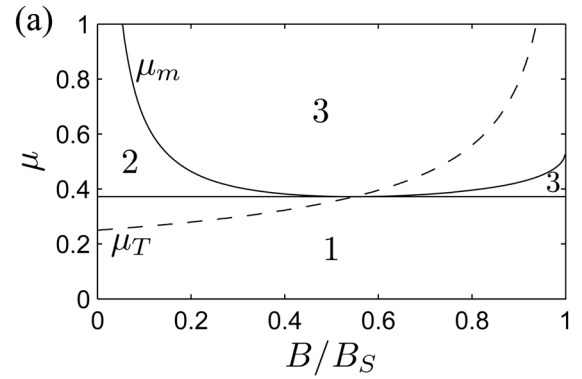

FIG. 2. (a) Parametric regions in the plane (B, μ) for ions of given energy E; the dashed line is the location of the minimum μ_T for different E. (b) Parametric regions in the plane (E, μ) at a given location B; the curve μ_m changes with B. In (a) and (b): region 1 is for ions to be collected, region 2 is for confined ions and regions 3 are devoid of ions. (c) Shape of the ion distribution function at one (B, ϕ) location, and for one particular energy; the limiting angle is $\theta_T = \sin^{-1}\sqrt{\mu_T/\mu_m}$, which is 90° at $B=B_T$ and 180° at $B=0$.

$$\mu_T(E) = \min\{\mu_m(B, E), \forall B\} \quad \text{at } B = B_T(E). \tag{7}$$

All ions of energy E with $w_\parallel>0$ that have $\mu<\mu_T(E)$ are collected at the wall, so that $w_\parallel<0$ ions exist only for $\mu>\mu_T$. Those with $\mu_T(E)<\mu<\mu_m(B, E)$ have a turning point along their axial trajectory. On the low-B side from the location $B=B_T(E)$, these ions could have $w_\parallel<0$ or $w_\parallel>0$, since their turning point is between them and the wall. Conversely, on the high-B side ($B>B_T$), no ions will exist, because the trajectories connect the wall with a turning point. This discussion is illustrated in Fig. 2, where we also illustrate the shape of the ion distribution for a single energy (and

hence a single w magnitude at a point): an incomplete spherical shell that evolves from a full sphere far from the wall to a forward half-sphere at B_T, to finally a limited forward cap at the sheath edge.

The differential volume in the velocity space in terms of E and μ, with symmetry about the magnetic line, is easily found to be $dEd\mu 2\pi B/(m_i^2|w_\parallel|)$, so that

$$n_i = \frac{2\pi B}{m_i^2} \int \int \frac{f_i(E,\mu)}{|w_\parallel|} dEd\mu, \tag{8}$$

where $f_i(E,\mu)$ is the ion distribution function in the three-dimensional velocity space. Then, the mean value of any quantity $\Phi(E,\mu)$ is

$$\langle \Phi \rangle = \frac{1}{n_i} \frac{2\pi B}{m_i^2} \int \int \Phi(E,\mu) \frac{f_i(E,\mu)}{|w_\parallel|} dEd\mu. \tag{9}$$

Examples of Φ are the axial velocity $w_\parallel$, as given by Eq. (5a), and the perpendicular kinetic energy, given as μB by Eq. (4b). Specific results will depend on the distribution f_i over the occupied portions of the (E,μ) map.

A. Solution for monoenergetic, initially isotropic ions

This case admits an analytical solution and provides guidance for more realistic cases. If all ions have the same energy $E=E_{i\infty}$,

$$f_i = \frac{m_i n_\infty}{4\pi} \left(\frac{m_i}{2E_{i\infty}} \right)^{1/2} \delta(E - E_{i\infty}), \tag{10}$$

where the normalization ensures $n_i=n_\infty$ where the full energy is kinetic (far from the wall). At locations with negative potential, f_i is still given by Eq. (10) provided ion trajectories connect to the distant plasma, but it is zero otherwise. Overall, therefore, f_i is not isotropic in the cusp.

The μ integration can be done directly. Notice that $\mu_T(E)$ and $B_T(E)$ are constants. Also, Eq. (5a) can be written as

$$w_\parallel = \pm \sqrt{\frac{2B}{m_i}(\mu_m - \mu)} \tag{11}$$

and so, for any limits μ_1, μ_2,

$$\int_{\mu_1}^{\mu_2} \frac{d\mu}{|w_\parallel|} = 2\sqrt{\frac{m_i}{2B}}[\sqrt{\mu_m - \mu_2} - \sqrt{\mu_m - \mu_1}]. \tag{12}$$

For $B > B_T$, the limits are $\mu_1=0$, $\mu_2=\mu_T$, and ions are counted only once, since all are traveling toward the wall. Substituting Eqs. (10) and (12) into Eq. (8),

$$n_i = \frac{n_\infty}{2} \left(\sqrt{1 - \frac{e\phi}{E}} - \sqrt{1 - \frac{e\phi + \mu_T B}{E}} \right), \quad \text{for } B > B_T. \tag{13}$$

For $B < B_T$, the μ range must be split. For $0 < \mu < \mu_T$, ions are counted once, but for $\mu_T < \mu < \mu_m$, a factor of two is needed to account for returning ions. The result is

$$n_i = \frac{n_\infty}{2} \left(\sqrt{1 - \frac{e\phi}{E}} + \sqrt{1 - \frac{e\phi + \mu_T B}{E}} \right), \quad \text{for } B < B_T. \tag{14}$$

The neutrality condition, Eq. (3), now reads

$$2\exp\left(\frac{e\phi}{kT_e}\right) = \sqrt{1 - \frac{e\phi}{E}} + \text{sign}(B_T - B)\sqrt{1 - \frac{e\phi + \mu_T B}{E}},$$

which can be solved for $B(\phi)$ (both signs), as

$$\frac{\mu_T B}{E} = 4\left(\sqrt{1 - \frac{e\phi}{E}} - e^{e\phi/kT_e} \right) e^{e\phi/kT_e}. \tag{15}$$

At the sheath edge ($\phi=\phi_S$, $B=B_S$), we must have $dB/d\phi=0$, which yields an implicit equation for $e\phi_S/kT_e$ as a function of E/kT_e:

$$\frac{kT_e}{2E} = \sqrt{1 - \frac{e\phi_S}{E}} \left(\sqrt{1 - \frac{e\phi_S}{E}} - 2e^{e\phi_S/kT_e} \right). \tag{16}$$

The reverse solution is explicit. Calling, for short $\psi_S = -e\phi_S/kT_e > 0$,

$$\frac{E}{kT_e} = \frac{4\psi_S e^{-2\psi_S} + 1 - 2\psi_S \pm 2e^{-\psi_S}\sqrt{4\psi_S^2 e^{-2\psi_S} + 1 - 2\psi_S}}{2(1 - 4e^{-2\psi_S})}. \tag{17}$$

With ϕ_S known, Eq. (15), expressed at S, determines the critical magnetic moment μ_T. The corresponding $B=B_T$ is that which makes $\mu_m(B)=\mu_T$. This completes the determination of $\phi(B)$.

We turn now to computing the macroscopic variables. The ion flux $\Gamma_i = n_i v_i$ with $v_i = \langle w_\parallel \rangle$, is due exclusively to ions with $\mu < \mu_T$. Since the μ integration is simply $\int_0^{\mu_T} w_\parallel |w_\parallel|^{-1} d\mu = \mu_T$, we obtain

$$\Gamma_i = \frac{n_\infty \mu_T}{\sqrt{8m_i E}} B, \tag{18}$$

showing the expected proportionality to B.

Even though all ions have the same total energy E, and, at one location, the same kinetic energy, the fact that their magnetic moments span a finite range implies a spread in both, their parallel and perpendicular kinetic energies [see Fig. 2(c)]. With the usual definitions for temperatures, $kT_{i\parallel} = \langle m_i c_\parallel^2 \rangle$ (with $c_\parallel = w_\parallel - v_i$) and $kT_{i\perp} = \langle m_i w_\perp^2/2 \rangle = B\langle \mu \rangle$, we must have

$$E = \frac{1}{2}m_i v_i^2 + \frac{1}{2}kT_{i\parallel} + kT_{i\perp} + e\phi \tag{19}$$

and so it is sufficient to calculate one of the temperatures, say $T_{i\perp}$. Using Eqs. (9)–(11), we obtain

$$\frac{kT_{i\perp}}{E} = \frac{1}{4} \frac{(B/E)^{3/2}}{(n_i/n_\infty)} \int \frac{\mu d\mu}{\sqrt{\mu_m - \mu}}, \tag{20}$$

where the limits of integration depend on whether B is less or more than B_T: for $B > B_T$, the limits are $0 < \mu < \mu_T$, whereas for $B < B_T$, we must add the contribution of ions with

$\mu_T < \mu < \mu_m$ and a factor of 2 must be included. The result for $T_{i\perp}$ is

$$\frac{kT_{i\perp}}{E} = \frac{1}{3}\frac{(B/E)^{3/2}}{(n_i/n_\infty)}$$
$$\times \left[\mu_m^{3/2} + \mathrm{sign}(B_T - B)\left(\mu_m + \frac{\mu_T}{2}\right)\sqrt{\mu_m - \mu_T}\right]. \quad (21)$$

When B approaches zero, it can be verified that both $T_{i\parallel}$ and $T_{i\perp}$ approach $T_{i\infty} = 2E/3$.

Due to the lack of symmetry of f_i with respect to the peculiar velocity $c_\parallel$, heat fluxes associated with axial transport of parallel and perpendicular random kinetic energy may occur (despite the lack of collisions). We define

$$q_{i\parallel} = n_i \langle m_i c_\parallel^3/2 \rangle, \quad (22)$$

$$q_{i\perp} = n_i \langle m_i w_\perp^2 c_\parallel/2 \rangle. \quad (23)$$

As with the calculation of the particle flux Γ_i, these are odd moments in $c_\parallel$, and so the μ integrations need to retain only the $0 < \mu < \mu_T$ part. After some algebra, we obtain

$$\hat{q}_{i\parallel} \equiv \frac{q_{i\parallel}}{n_\infty kT_e c_{s0}} = 0, \quad (24)$$

$$\hat{q}_{i\perp} \equiv \frac{q_{i\perp}}{n_\infty c_{s0} kT_e} = \frac{\hat{B}^2 \hat{\mu}_T^2}{2^{5/2}\hat{E}^{1/2}} - \hat{\Gamma}_i \hat{T}_{i\perp}. \quad (25)$$

Figure 3 shows the relevant plasma parameters. Variables in Fig. 3 and in Eq. (25) are normalized as

$$\hat{B} = \frac{B}{B_S}, \quad \psi = -\frac{e\phi}{kT_e}, \quad \hat{T} = \frac{T}{T_e}, \quad \hat{E} = \frac{E}{kT_e}, \quad \hat{\mu} = \frac{\mu B_S}{kT_e},$$
$$\quad (26)$$
$$\hat{n} = \frac{n}{n_\infty}, \quad \hat{v} = \frac{v}{c_{s0}}, \quad \hat{\Gamma} = \frac{\Gamma}{n_\infty c_{s0}}, \quad \hat{q} = \frac{q}{n_\infty c_{s0} kT_e},$$

where $c_{s0} = \sqrt{kT_e/m_i}$ is the cold-ion Bohm velocity, or isothermal speed of sound.

An important result is that, for all values of E/kT_e, the presheath potential remains in a narrow range, from $-e\phi_S/kT_e = 0.5$ when $E/kT_e = 0$ to $-e\phi_S/kT_e = \ln 2$ when $E/kT_e \gg 1$, with a shallow maximum of 0.7512 when $E/kT_e = 0.7588$. Notice also in Fig. 3 the decay of $T_{i\parallel}$ as the wall is approached, and conversely, the increase in $T_{i\perp}$, particularly when E/kT_e is small. As one might expect given this positive gradient of $T_{i\perp}$, the heat flux $q_{i\perp}$ is seen to be negative (away from the wall); but it must be kept in mind that this heat flux is a consequence of the collisionless distortions of f_i, and consequently the mean-free-path argument for a proportionality to the negative temperature gradient does not apply. The heat flux $q_{i\parallel}$, giving the random transport of parallel random velocity, is found to be exactly zero in this model; this is in spite of a clear lack of symmetry of the ion distribution about the mean parallel velocity, and no explanation has been identified for this behavior.
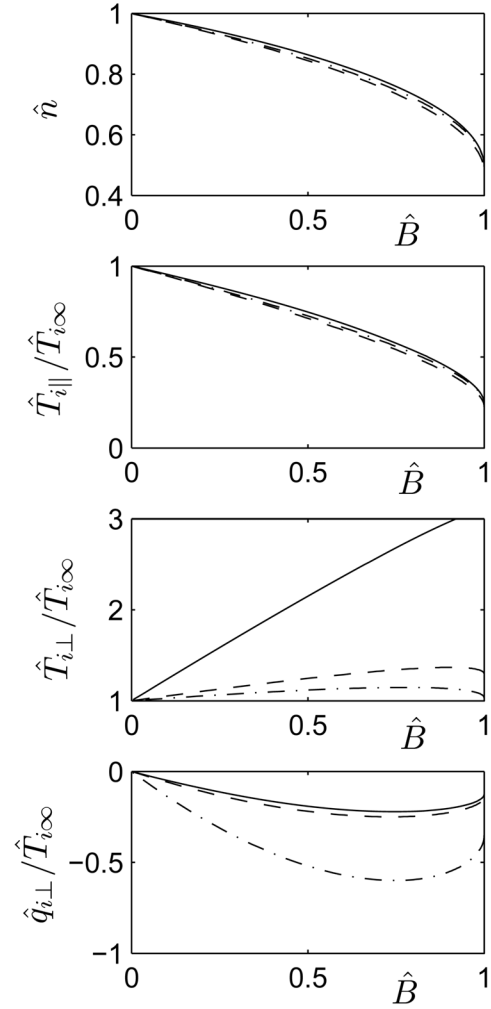

FIG. 3. Spatial profiles (in terms of B) of main magnitudes for a monoenergetic population of ions. Lines are for $\hat{T}_{i\infty} \equiv T_{i\infty}/T_e = 0.1$ (solid), 1 (dashed), and 10 (dash-and-dot).

B. Ions that are Maxwellian far from the wall

Since the distribution f_i is a function of the constants of the motion, we have in this case

$$f_i = n_\infty \left(\frac{m_i}{2\pi kT_{i\infty}}\right)^{3/2} e^{-(E/kT_{i\infty})}, \quad (27)$$

whenever an ion trajectory connects to the distant Maxwellian plasma. Where that connection does not happen, but a magnetic connection exists to the wall, we have $f_i = 0$. The discussion in Sec. II still applies, and the integrations with respect to μ for the various moments are subject to the same considerations at each energy E as those discussed in Sec. II A for the single-energy case.

It will be recalled that for the even moments (such as n_i, $T_{i\parallel}$, $T_{i\perp}$), the single-energy results depend on whether B is less or more than $B_T(E)$, the location at which the turning point magnetic moment μ_m reaches its minimum value $\mu_T(E)$ for the given energy. Examination of Fig. 2 shows that if we now fix a value of B/B_S and vary the energy E, the

TABLE I. Ranges of integration for even moments.

Energy range	B range	Range for μ integration
$E < E_T(B)$	$B > B_T(E)$	$\int_0^{\mu_T(E)}(\ldots)d\mu$
$E > E_T(B)$	$B < B_T(E)$	$\int_0^{\mu_T(E)}(\ldots)d\mu + 2\int_{\mu_T(E)}^{\mu_m(E,B)}(\ldots)d\mu$

correspondences of Table I occur, where $E_T(B)$ is the inverse function of $B_T(E)$. For the odd moments (such as Γ_i, $q_{i\parallel}$, and $q_{i\perp}$) the μ range is $0 < \mu < \mu_T(E)$, as before.

The calculations of Sec. II A can be extended to the Maxwellian case using Eqs. (8) and (9) with the distribution of Eq. (27) and integration ranges of Table I. We next apply these ideas to the ion density calculation, with the result, using Eqs. (13) and (14),

$$\frac{n_i(B)}{n_\infty} = \frac{1}{\sqrt{\pi}(kT_{i\infty})^{3/2}} \int_0^\infty e^{-(E/kT_{i\infty})}(\sqrt{E - e\phi}$$
$$+ \operatorname{sign}[E - E_T(B)]\sqrt{E - e\phi - \mu_T(E)B})dE. \quad (28)$$

The difficulty that now arises is that the calculation of $\mu_T(E)$, as the minimum of $\mu_m = (E - e\phi)/B(\phi)$ requires knowledge of the $\phi(B)$ function, which itself is to be found by imposing quasineutrality, i.e., Eq. (3). This cannot be done analytically, but a numerical iteration process can be used to solve the problem. On fixed grids of $\hat{B}$ and $\hat{E}$, the normalized potential $\psi(\hat{B}) = -e\phi/kT_e$ is initialized using results from the monoenergetic case. For each $\hat{E}$, the quantity $\hat{\mu}_m(\hat{E}, \hat{B})$ is computed versus $\hat{B}$, and its minimum, $\hat{\mu}_T(\hat{E})$ is determined, together with the location $\hat{B} = \hat{B}_T(\hat{E})$ where it occurs. This also determines the dividing energy $\hat{E}_T(\hat{B})$, and the integrations of Eq. (28) can now be performed to find $\hat{n}_i(\hat{B})$. Imposing neutrality, Eq. (2) yields a new $\psi(\hat{B})$ profile, and this is repeated to convergence; under-relaxation is actually required, especially at low values of $T_{i\infty}/T_e$.

Once $\mu_T(E)$ and $E_T(B)$ are known, all the relevant moments can be computed. The profiles of density, temperatures and heat fluxes, for $T_{i\infty}/T_e = 0.1$, 1, and 10, are displayed in Fig. 4, and comparison to Fig. 3 shows very similar shapes and magnitudes for the Maxwellian and monoenergetic cases, with the exception of a nonzero $q_{i\parallel}$ in the Maxwellian case. The similarity is shown more clearly in Fig. 5, where the particular values at the sheath edge are compared between the two models for a wide range of $T_{i\infty}/T_e$.

In closing, it is worth emphasizing the very different ways in which the magnetic cusp and its self-consistent presheath potential affect electrons and ions. Because of their almost total confinement, the electron distribution remains Maxwellian at a constant temperature. On the other hand, ions are collected or neutralized at the wall, and so their distribution tends to become one-sided and their parallel and perpendicular temperatures change as the wall is approached. Of course, this asymmetric behavior is not peculiar of this problem: a comparable behavior is found in the well-known, unmagnetized Tonks–Langmuir problem,[15] where ionization plays for ions the role of the cusp convergence here.
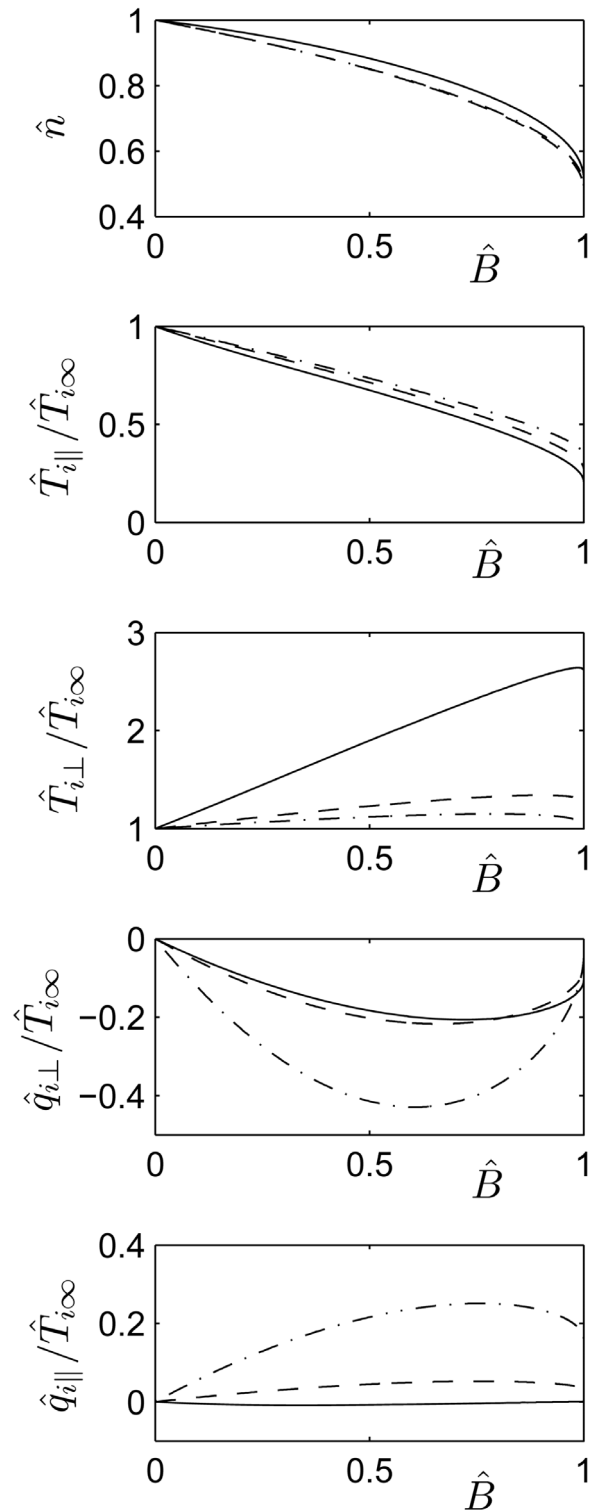

FIG. 4. Spatial profiles (in terms of B) of main magnitudes for a Maxwellian population of ions. Lines are for $\hat{T}_{i\infty} = 0.1$ (solid), 1 (dashed), and 10 (dash-and-dot).

III. MOMENTS OF THE ION DISTRIBUTION AND CONSERVATION LAWS

An independent check on our results can be obtained from the fluid, or moment equations. These are obtained by the classical method of multiplication of Boltzmann's equation times a sequence of functions $\Phi(\vec{w})$, followed by inte-
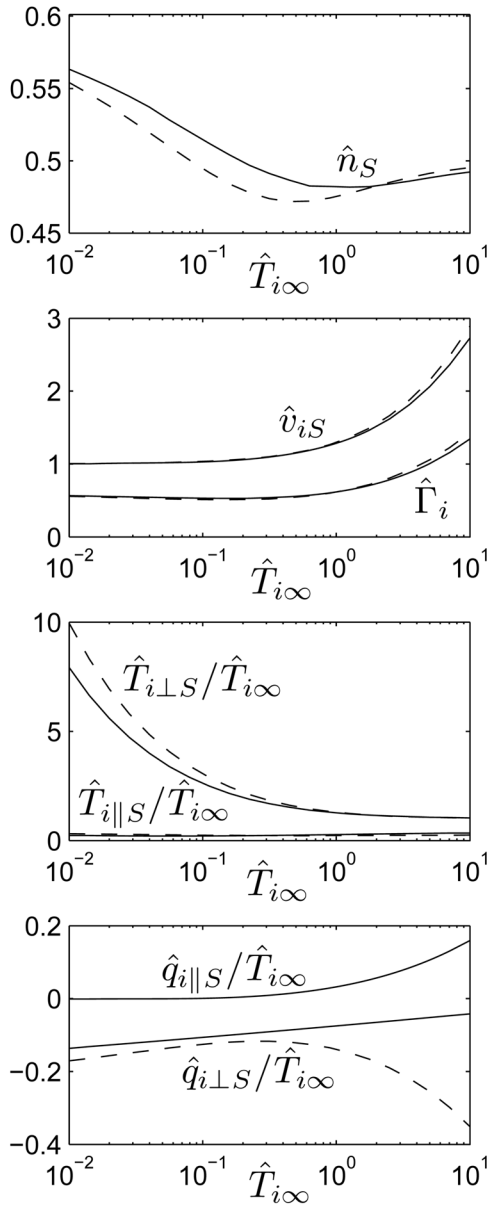
FIG. 5. Parametric response at the sheath edge S for Maxwellian (solid) and monoenergetic (dashed) populations of ions in terms of their unperturbed temperature. For the monoenergetic population, $q_{i\parallel}=0$.

gration over all $\vec{w}$. For a strongly magnetized species, with no collisions, Ramos[16] gives the results corresponding to $\Phi=1$, $m_i\vec{w}$, $m_i\vec{w}\vec{w}$, and $m_i\vec{w}\vec{w}\vec{w}$, the last two of these being tensors of order 2 and 3, respectively. To the lowest order in the Larmor radius, all vector fluxes are along the magnetic field, and the kinetic energy splits naturally into parallel $(m_i w_\parallel^2/2)$ and perpendicular $(m_i w_\perp^2/2)$ components. One thus obtains one continuity equation, one momentum equation along the magnetic field and one equation for each of the pressures

$$P_{i\parallel} = n_i k T_{i\parallel} = mn_i\langle c_\parallel^2\rangle,$$

$$P_{i\perp} = n_i k T_{i\perp} = mn_i\langle w_\perp^2\rangle/2. \tag{29}$$

Ramos obtains in addition two equations for the third-order quantities $q_{i\parallel}$ and $q_{i\perp}$, defined as in Eqs. (22) and (23). It is characteristic of this sequence that the equation for a moment of order n involves one or more moments of order $n+1$, so that no complete description is generally possible with a finite number of moment equations. Thus, for example, the equations for $q_{i\parallel}$ and $q_{i\perp}$ involve the energy-weighted and parallel energy-weighted stress tensor components

$$r_\parallel = \tfrac{1}{2}nm\langle c^2 c_\parallel^2\rangle, \quad r_\perp = \tfrac{1}{4}nm\langle c^2 c_\perp^2\rangle, \quad r_B\perp = \tfrac{1}{4}nm\langle c_\parallel^2 c_\perp^2\rangle,$$

with $\vec{c}=\vec{w}-\vec{v}_i$. Ramos expresses his results in general vector notation, valid for arbitrary geometry, and including time-dependent effects. We will particularize his equations for the steady state and take advantage of the fact that all spatial derivatives appearing are in the magnetic direction (along the z-axis).

For any vector $\vec{a}$ directed along the magnetic field we have

$$\nabla \cdot \vec{a} = \nabla \cdot \left(\frac{a}{B}\vec{B}\right) = \vec{B} \cdot \nabla\left(\frac{a}{B}\right) = B\frac{d}{dz}\left(\frac{a}{B}\right), \tag{30}$$

where the last equality implies a quasi-1D geometry. In particular, the ion continuity equation is $\nabla\cdot(n_i\vec{v}_i)=0$, and this can be written, from Eq. (30), as

$$\frac{d}{dz}\left(\frac{n_i v_i}{B}\right) = \frac{d}{dz}\left(\frac{\Gamma_i}{B}\right) = 0, \tag{31}$$

which is, as noted, satisfied by our kinetic results [Eq. (18) and Fig. 3].

The ion momentum equation along the magnetic field can be similarly reduced to

$$m_i n_i v_i \frac{dv_i}{dz} + \frac{dP_{i\parallel}}{dz} + (P_{i\perp} - P_{i\parallel})\frac{d\ln B}{dz} + en_i\frac{d\phi}{dz} = 0, \tag{32}$$

showing explicitly the magnetic mirror effect of an anisotropic pressure tensor. With some rearrangement, Eq. (32) can be put in a Bernoulli-like form that will be of use later:

$$\frac{dH_i}{dz} = \frac{1}{2v_i^3}\frac{d}{dz}(kT_{i\parallel}v_i^2) + B\frac{d}{dz}\left(\frac{kT_{i\perp}}{B}\right), \tag{33}$$

where

$$H_i = \tfrac{1}{2}m_i v_i^2 + \tfrac{3}{2}kT_{i\parallel} + kT_{i\perp} + e\phi. \tag{34}$$

Notice that the "expansion work" part of the total enthalpy per particle H_i is $kT_{i\parallel}$, and the "internal energy" part is $kT_{i\perp}+kT_{i\parallel}/2$. Equation (33) indicates that this total enthalpy is conserved only if the terms on its right hand side are zero.

The two equations for $P_{i\parallel}$ and $P_{i\perp}$ (or for $T_{i\parallel}$ and $T_{i\perp}$) are adapted from Eqs. (31) and (32) of Ref. 16:

$$P_{i\parallel}\vec{v}_i \cdot \nabla \ln\left(\frac{B^2 P_{i\parallel}}{n_i^3}\right) + 2\vec{b}\cdot\nabla q_{i\parallel} + 2(q_{i\perp}-q_{i\parallel})\vec{b}\cdot\nabla\ln B = 0,$$

$$\tag{35}$$

$$P_{i\perp}\vec{v}_i \cdot \nabla \ln\left(\frac{P_{i\perp}}{Bn_i}\right) + \vec{b}\cdot\nabla q_{i\perp} + 2q_{i\perp}\vec{b}\cdot\nabla\ln B = 0, \tag{36}$$

where $\vec{b}=\vec{B}/B$. When the heat fluxes $q_{i\parallel}$ and $q_{i\perp}$ are neglected, these equations reduce to the steady-state form of the CGL double-adiabatic laws[14]

$$\frac{B^2 P_{i\parallel}}{n_i^3} \equiv \frac{B^2 k T_{i\parallel}}{n_i^2} = \text{const} \quad (\text{or } T_{i\parallel} v_i^2 = \text{const}), \qquad (37)$$

$$\frac{P_{i\perp}}{B n_i} \equiv \frac{k T_{i\perp}}{B} = \text{const}, \qquad (38)$$

which according to Eq. (33) would also guarantee H_i =const. Reference to our kinetic results of Sec. II B will show that these adiabatic laws are not very good approximations, especially when $T_{i\infty}/T_e$ is not very small.

If $(q_{i\parallel}, q_{i\perp})$ are retained in Eqs. (35) and (36), and the quasi-1D approximation is invoked, two new quantities are conserved along z. First, direct manipulation of Eq. (36) leads to the simple exact form

$$\frac{d}{dz}\left(\frac{k T_{i\perp} + q_{i\perp}/\Gamma_i}{B}\right) = 0, \qquad (39)$$

which extends CGL's Eq. (38) by adding to the mean perpendicular energy its axial transport rate per unit particle flux. An alternative interpretation of Eq. (39) is that the total (convected plus conducted) heat transported by a variable-area flux tube remains constant, a result that could have been anticipated on physical grounds.

Now, Eq. (35) can be similarly manipulated to the form

$$\frac{d}{dz}(k T_{i\parallel} v_i^2) = -\frac{2 v_i B}{n_i}\left[\frac{d}{dz}\left(\frac{q_{i\parallel}}{B}\right) + \frac{q_{i\perp}}{B^2}\frac{dB}{dz}\right]. \qquad (40)$$

This does not directly yield a conservation law, but it does when substituted, together with Eq. (39), into Eq. (33):

$$\frac{d}{dz}\left(H_i + \frac{q_{i\parallel} + q_{i\perp}}{\Gamma_i}\right) = 0, \qquad (41a)$$

where H_i is the ordinary total ion enthalpy, Eq. (34). Once again, this adds to the total ion mean kinetic energy its total flux per unit particle flux, and it defines a new conserved quantity, a sort of generalized ion enthalpy,

$$H_i^* = \frac{1}{2} m_i v_i^2 + \frac{3}{2} k T_{i\parallel} + k T_{i\perp} + \frac{q_{i\parallel} + q_{i\perp}}{\Gamma_i} + e\phi. \qquad (41b)$$

As in the case of Eq. (39), Eq. (41a) could also be interpreted as stating that the total enthalpy flux *per unit area*, including now both heat fluxes, is conserved in the magnetic direction.

Equations (39) and (41a) have been checked against the kinetic results of Secs. II A and II B, and found to be precisely satisfied by both monoenergetic and Maxwellian ions and are, to our knowledge, new results. The relative weight of the heat fluxes that are neglected in the CGL approximation, Eqs. (37) and (38), is displayed in Fig. 6, where they are seen to be generally of the same order as the convected thermal energy fluxes. The potential utility of Eqs. (39) and (41) depends on some approximate closure scheme that would relate the heat fluxes to the lower order moments or their derivatives. One such scheme has been developed by Ramos,[16] who proceeded by first obtaining evolution equations for $q_{i\parallel}$ and $q_{i\perp}$ and then deriving approximate closure relations between the fourth order moments, $r_\parallel$, $r_\perp$, and $r_{B\perp}$,
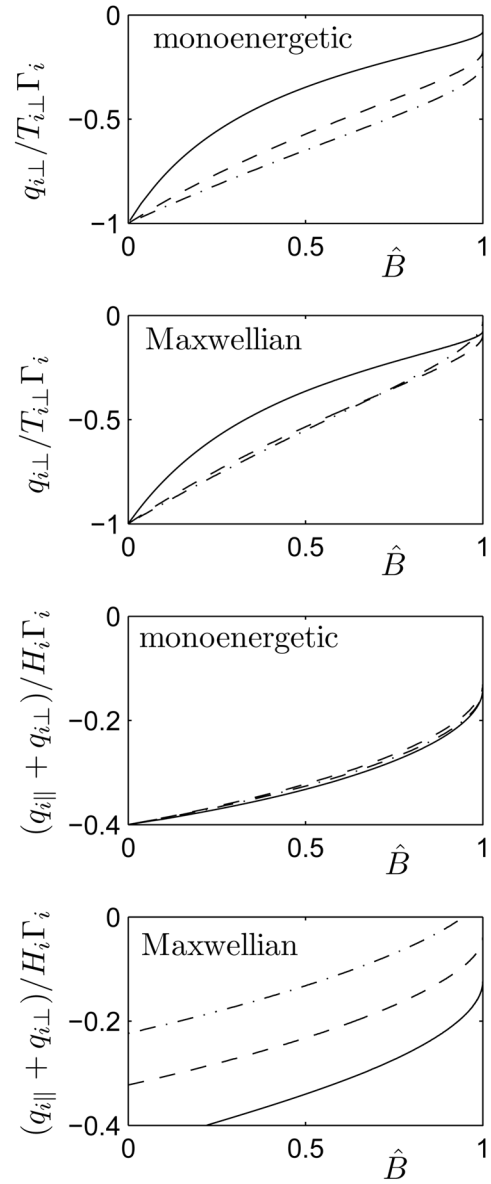

FIG. 6. Relative weight of the heat fluxes in the two energy conservation equations of the quasi-1D model for monoenergetic and Maxwellian ion populations, and $\hat{T}_{i\infty} = 0.1$ (solid), 1 (dashed), and 10 (dash-and-dot).

and the second-order moments, and $P_{i\perp}$. The accuracy of these closures could be investigated by comparison to our kinetic results, but this remains to be done.

The Bohm criterion of the presheath-sheath asymptotic theory, applied to a macroscopic formulation of a plasma accelerated from rest, establishes that the presheath-sheath edge S is a singular (or sonic) point of the quasineutral equations for ions. That sonic velocity, v_{iS}, is known as the Bohm velocity, and is plotted in Fig. 5. Using Eqs. (2), (31), and (40) in order to eliminate the derivatives of ϕ, n, and $T_{i\parallel}$ in Eq. (32), one has

$$(m_i v_i^2 - k T_e - 3 k T_{i\parallel}) n_i \frac{dv_i}{dz} - 2\frac{dq_{i\parallel}}{dz}$$

$$= -[2(q_{i\parallel} - q_{i\perp}) + v_i(P_{i\perp} + P_e)]\frac{d\ln B}{dz}, \qquad (42)$$
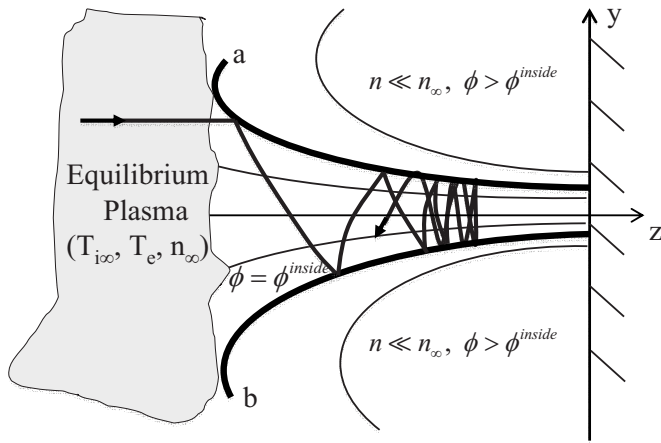
FIG. 7. Schematic showing the trajectory of an ion that is electrostatically confined by the potential depression in the "channel" bounded by the last magnetic lines, a and b, that connect to the equilibrium distant plasma. The region outside this channel is nearly devoid of electrons, and at a higher potential due to some small ion population that spills from the channel.

as the *exact* equation for the evolution of v_i. Then, if $q_{i\parallel}(z)=0$, as for a monoenergetic ion population, the Bohm velocity satisfies

$$v_{iS}=c_s \equiv \sqrt{k(T_e+3T_{i\parallel S})/m_i},$$

in agreement with the hydrodynamic Bohm criterion.[17] For a general ion distribution function, the functional form of v_{iS} depends on the expression of the closure equation for $dq_{i\parallel}/dz$. If the *exact* form of that equation were known and used together with Eq. (42), the resulting sonic condition would agree with the kinetic Bohm criterion,[18] $\langle w_\parallel^{-2}\rangle_S = m_i/kT_e$, which implies that $v_{iS} > \sqrt{kT_e/m_i}$ (Ref. [19]). For the Maxwellian ion population here the numerical results show that v_{iS}/c_s decreases slowly (from 1) with $T_{i\infty}/T_e$ increasing from 0, having $v_{iS}/c_s \simeq 0.95$ for $T_{i\infty}/T_e=1$.

IV. NONMAGNETIZED IONS, MAGNETIZED ELECTRONS

In many practical cases, the ion gyro radius is comparable or larger than the lateral dimension of the magnetic "duct," while the electron gyro radius is much smaller than this dimension. In the limit, ions react only to electrostatic fields, which are themselves set up by the small deviations from neutrality between them and the magnetically guided ions. Specifically, if there is one limiting magnetic line, like a or b, in Fig. 7, beyond which no connection is made to the equilibrated plasma, the B-lines beyond this will be drained of electrons, and ions will only penetrate a small distance into this outer region, due to the self-consistent high potential they will create there. Wall probe data of Fig. 1(c), recently obtained near the cusps in a DCF thruster[5] show the existence of potential "canyons" similar to that sketched in Fig. 7 in front of each of them.

Ions moving toward the wall along one of these low-potential channels will bounce repeatedly off of its sidewalls, and their trajectories will rotate by roughly twice the side-wall angle in each such bounce. As sketched in Fig. 7, this may eventually cause the ion to turn back away from the

wall, similarly to what would happen in a magnetic mirror. This similarity with a magnetic mirror prompts the question whether an adiabatic invariant analogous to the magnetic moment would exist in the electrostatic case. Within the same limitations (slow convergence of the B-lines), this can be answered in the affirmative using the known adiabatic invariance of the action integral[20] $J=\oint pdq$, where q is a cyclic or quasi-cyclic degree of freedom, p is its conjugate momentum, and the integral is taken along a full cycle (or quasicycle). In our case, assuming a line-cusp two-dimensional (2D) geometry, q is the lateral displacement y of an ion from the channel centerline, and $p=m_i\dot{y}$ is the lateral momentum, so that

$$J=\oint pdq=4\int_0^{y_2}m_i\dot{y}dy=4\sqrt{2em_i}\int_0^{y_2}\sqrt{\phi(y_2)-\phi(y)}dy,$$
(43)

where y_2 is a turning point, and lateral symmetry has been assumed.

For concreteness, consider the potential

$$\phi=\phi_c+(\phi_2-\phi_c)(y/y_2)^n$$
(44)

with $\phi_c=\phi(0)$ and n a fitting exponent. Direct substitution in Eq. (43) leads to $J=4p_n\sqrt{2em_i(\phi_2-\phi_c)}y_2$, with $p_n=\int_0^1 \times(1-\eta^n)d\eta$. To estimate y_2, the lateral excursion of an ion, assume next that the potential at $y=h(z)$ (the half-width of he potential channel) is half-way up to the external potential ϕ^{out}. Substituting in Eq. (44) leads to

$$y_2=h\left(2\frac{\phi_2-\phi_c}{\phi^{out}-\phi_c}\right)^{1/n}$$

and hence to

$$J=4p_n\sqrt{2em_i}\left(\frac{2}{\phi^{out}-\phi_c}\right)^{1/n}h(\phi_2-\phi_c)^{(2+n)/2n}.$$

We notice that $e(\phi_2-\phi_c)=m_i\dot{y}^2(0)/2$, the ion lateral energy at centerline crossing, which itself can be shown to be a constant fraction of the *average* kinetic energy $\langle m_i\dot{y}^2/2\rangle$. We therefore conclude that the quantity

$$h\langle m_iw_\perp^2/2\rangle^{(2+n)/2n}$$
(45)

is an adiabatic invariant. Since $hB=$constant in our 2D geometry, this can be finally expressed as

$$\varepsilon \equiv \langle m_iw_\perp^2/2\rangle B^{-2n/(2+n)} = \text{invariant}.$$
(46)

Two limits stand out:

(a) For a *parabolic* potential well ($n=2$), $\varepsilon=\langle m_iw_\perp^2\rangle/2B$, which is identical to μ, the magnetic moment.

(b) For a *flat-bottom* potential well with steep walls ($n\to\infty$),

$$\varepsilon=\langle m_iw_\perp^2\rangle/2B^2,$$
(47)

which shows a more rapid variation of the perpendicular energy with B. The difference can be traced to the fact that ions are able to penetrate farther into the outside potential when the wall is "soft," i.e., as the channel narrows towards the wall and oscillating ions gain

transverse energy, their oscillation amplitude y_2 tends to overshoot h, causing a reduction in the effective convergence rate. This is then reflected in the less steep increase of the ion transverse energy ($\propto B$ rather than $\propto B^2$).

Given the smallness of the Debye length in most cases of interest, the square well appears to be the more realistic choice, subject, of course to our assumption that electrons are sharply confined to a well-defined channel. More realistic electron models would require a refinement of this assumption, involving detailed consideration of the distant plasma and its connection to the weak part of the field.

The importance of Eq. (47) or Eq. (46) is that all the results obtained in Secs. II A and II B for magnetized ions are immediately applicable to the opposite, unmagnetized case, with only an axial rescaling: B/B_S is to be replaced everywhere by $(B/B_S)^2$, or, more generally, $(B/B_S)^{2n/(2+n)}$. In particular, this shows that the ion flux Γ_i is nearly unaffected by the cusp. The cusp does limit the width of the wall exposed to this flux, perhaps to a few gyro radii,[11] but that is outside the scope of the present model.

As a final note, if the geometry is that of a point-cusp instead of a line cusp, the arguments leading to Eq. (45) still apply, up to some constants, but we now have $h^2 B = \text{const}$ instead of $hB = \text{const}$. In that case, a potential profile with a flat bottom implies that the electrostatic adiabatic constant is actually the same as the magnetic moment, i.e., $\varepsilon = \mu = \langle m_i w_\perp^2 \rangle / 2B$. Thus, for a point-cusp, the plasma properties are identical with magnetized and with nonmagnetized ions.

V. CONCLUSIONS

A kinetic model has been formulated for plasmas in a magnetic cusp, where electrons are strongly magnetized and isotropic in energy, and ions are either strongly magnetized or nonmagnetized, but strongly guided by the self-consistent electrostatic field that results from their slight separation from the magnetized electrons. The structure along the cusp centerline, which is fully correlated by the local magnetic field strength, is very similar to that of an ordinary presheath, and so are the sheath entrance potential and ion flux. The wall-protecting function of the cusp is therefore associated only with its ability to exclude ion fluxes to regions not magnetically connected to the distant "feeder" plasma. Ana-lytical results are found for a monoenergetic ion population, and numerical results are obtained for a Maxwellian plasma far from the wall, in both cases for a wide range of electron/ion energies. The results are shown to satisfy the leading ion moment equations, including two new conservation laws that, for a quasi-1D, stationary plasma, exactly generalize the classical CGL constants when the ion heat fluxes are nonzero.

[1] D. G. Courtney and M. Martinez-Sanchez, *Proceedings of the 30th International Electric Propulsion Conference*, Florence, Italy, September 2007, Paper IEPC-2007-39.
[2] D. G. Courtney, SM thesis, MIT, 2008.
[3] D. G. Courtney, P. Lozano, and M. Martinez-Sanchez, *Proceedings of the 44th Joint Propulsion Conference*, Hartford, MA, July 2008, Paper AIAA-2008-4631.
[4] S. R. Gildea, S. R. Nakles, M. Hargus, and M. Martinez-Sanchez, *Proceedings of the 31st International Electric Propulsion Conference*, Ann Arbor, MI, September 2009, Paper IEPC-2009-259.
[5] T. Matlock, S.R. Gildea, P. Lozano, and M. Martinez-Sanchez, *Proceedings of the 46th Joint Propulsion Conference*, Nashville, TN, July 2010, Paper AIAA-2010-7104.
[6] Y. Raitses and N. J. Fisch, Phys. Plasmas **8**, 2579 (2001).
[7] A. Smirnov, Y. Raitses, and N. J. Fisch, Phys. Plasmas **14**, 057106 (2007).
[8] G. Kornfeld, N. Koch, and G. Coustou, *Proceedings of the 28th International Electric Propulsion Conference*, Toulouse, France, March 2003, Paper IEPC-2003-134.
[9] H. P. Harmann, N. Koch, and G. Kornfeld, *Proceedings of the 30th International Electric Propulsion Conference*, Florence, Italy, September 2007, Paper IEPC-2007-114.
[10] D. M. Goebel and I. Katz, *Fundamentals of Electric Propulsion: Ion and Hall Thrusters* (Wiley, New York, 2008).
[11] K. N. Leung, N. Hershkowitz, and K. R. MacKenzie, Phys. Fluids **19**, 1045 (1976).
[12] R. A. Bosch and R. L. Merlino, Phys. Fluids **29**, 1998 (1986).
[13] C. Koch and G. Matthieussent, Phys. Fluids **26**, 545 (1983).
[14] G. F. Chew, M. L. Goldberger, and F. E. Low, Proc. R. Soc. London, Ser. A **236**, 112 (1956).
[15] L. Tonks and I. Langmuir, Phys. Rev. **34**, 876 (1929).
[16] J. J. Ramos, Phys. Plasmas **10**, 3601 (2003).
[17] K. U. Riemann, J. Phys. D: Appl. Phys. **24**, 493 (1991).
[18] E. R. Harrison and W. B. Thompson, Proc. Phys. Soc. London **74**, 145 (1959).
[19] E. Ahedo, R. Santos, and F. Parra, Phys. Plasmas **17**, 073507 (2010).
[20] H. Goldstein, *Classical Dynamics* (Addison-Wesley, Reading, MA, 1953).